J. Astrophys. Astr. (2018) 39:30
https://doi.org/10.1007/s12036-018-9522-9

Multiband optical–IR variability of the blazar PKS 0537–441

XIAO-PAN LI[1,*], LI-SHA WANG[1], CHENG YANG[2], HAI-YAN YANG[1], LI ZHOU[1], GUANG-YANG XU[1], YU-QIONG SHAN[1], JIE LIU[1], YU-HUI LUO[1] and LI ZHANG[3,4]

[1]Department of Physics, Zhaotong University, Zhaotong 657000, China.
[2]College of Optoelectronic and Communication Engineering, Yunnan Open University, Kunming 650223, China.
[3]School of Foreign Language, Xiamen University, Xiamen 361005, China.
[4]School of Foreign Language, Zhaotong University, Zhaotong 657000, China.
*Corresponding author. E-mail: lxpzrc@163.com

MS received 17 November 2017; accepted 2 March 2018; published online 20 April 2018

Abstract. We have reconsidered the simultaneous and homogeneous optical–IR light curves and the corresponding spectral indices curve of the blazar PKS 0537–441 from January 2011 to May 2015. All the curves show significant fluctuations on various timescales, and the flux variations seem to be more pronounced towards the IR bands. The relation between average fluxes and spectral indices reveals the existence of redder-when-brighter (RWB) and bluer-when-brighter (BWB) trends at different flux levels, along with a long-term achromatic trend and a mild RWB trend on short-term timescales. Cross-correlation analyses present an energy-dependent time delay that the lower-frequency variations follow higher-frequency ones by a few weeks and a hysteresis pattern between spectra and fluxes. Our analysis reveals some potential coherence between low-energy-peaked BL Lacs (LBLs) and FSRQs, and indicates that the observed flux variability and spectral changes could be due to the superposition of a dominant jet emission, an underlying thermal contribution from a more slowly varying disk and/or other geometric effects under the shock-in-jet scenario.

Keywords. Galaxies—active—BL lacertae objects—general—BL lacertae objects—individual—PKS 0537–441.

1. Introduction

Multi-wavelength studies of blazars play an important role in understanding the properties of their relativistic jets, central engines and radiative transfer processes. In the most acceptable scenarios of blazars, their non-thermal continuum emission across the entire electromagnetic spectrum originates from a relativistic jet that aligned with the line of sight, and their spectral energy distributions (SEDs) exhibit a characteristic broad double-peaked structure with the low-energy peak between infrared (IR) to ultraviolet (UV)/X-rays and the high-energy peak in the MeV–TeV band (e.g., Urry & Padovani 1995; Ulrich *et al.* 1997). The low-energy humps of the SEDs are associated with the synchrotron radiation coming from the jet relativistic electrons (or pairs), while the high-energy humps can be modelled with the leptonic and hadronic scenarios. The leptonic model attributes the high-energy emission to inverse Compton (IC) processes with seed photons coming from the synchrotron process (synchrotron self-Compton (SSC); e.g. Maraschi *et al.* 1992; Böttcher 2007) or from an external region (EC; e.g. Celotti *et al.* 2007; Ghisellini *et al.* 2014), such as the accretion disk, broad line region (BLR) or the dust torus, while the hadronic model attributes it to the proton synchrotron and/or hadron–photon-initiated cascades (e.g., Mannheim 1998; Böttcher 2007).

The blazar PKS 0537–441, at redshift $z = 0.896$, is a well studied southern source and detected in all accessible spectral wavebands. This source is usually classified as a low-energy-peaked BL Lac based on its synchrotron peak. The overall SEDs in different intensity states and spectral variability have been discussed in detail by Pian *et al.* (2002), while the long-term multi-wavelength observations obtained from microwaves through γ-rays by different instruments were reported in D'Ammando *et al.* (2013). In

the IR/optical bands considered, several telescopes were employed to monitor this source in their observing schedules. For example, the Rapid Eye Mount telescope (REM, Zerbi *et al.* 2001) located at the ESO La Silla observatory (Chile) monitors variable source simultaneously in IR (*JHK*) and optical (*VRI*) bands, and the Small and Medium Aperture Research Telescope System program (SMARTS[1]) organized by Yale University monitors the *Fermi*-LAT source densely. Based on the REM data, a short timescale of about 25 min in the IR *J* and optical *V* bands has been identified (Impiombato *et al.* 2011; Zhang *et al.* 2013), and a bluer-when-bright (BWB) colour behaviour on diverse timescale has also been discussed (Li *et al.* 2015). Recently, with the integrated *R*-band light curve obtained by combining REM and SMARTS data, Sandrinelli *et al.* (2016) detected a quasi-periodic oscillation (QPO) of about 140 d, which is relevant to a QPO of about 280 d found in their Fermi γ-ray light curve in a high state. Li *et al.* (2017) investigated the simultaneous variability, cross-correlation and spectral behaviour of PKS 0537–441 in NIR/optical, UV and X-ray wavebands on the basis of the REM and Swift observations in 2009–2011.

In this paper, we focus on the SMARTS optical–IR variability of PKS 0537–441. We describe the simultaneous observations and temporal variability in section 2. In sections 3 and 4, we report the results of the spectral behaviours and the cross-correlation analysis, respectively. We draw the summary in section 5.

2. Observations and temporal variability

The SMARTS consortium operates four 1m-class (1.5-m, 1.3-m, 1.3-m and 0.9-m) telescopes located at Cerro Tololo Inter-American Observatory (CTIO) in Chile to monitor *Fermi*-LAT source in the *B*, *V*, *R*, *J*, and *K* bands. PKS 0537–441 was regularly monitored with the ANDICAM instrument mounted on the SMARTS 1.3 m telescope from MJD 55590 to MJD 57144. The ANDICAM has the capability to take optical and IR data simultaneously with a dichroic that feeds an optical CCD and an IR imager. We obtained the photometric optical–IR data from the SMARTS publically accessible database, corrected them for Galactic extinction with $E(B-V) = 0.032$ (Schlafly & Finkbeiner 2011) and the extinction law of Cardelli *et al.* (1989) and converted theoptical–IR magnitudes to absolute fluxes using the zero points in Bessell *et al.* (1998). As for more comprehensive description of the SMARTS project and data reduction, refer to Bonning *et al.* (2012).

Figure 1 represents the optical–IR light curves and spectral indices curve of this source. The optical–IR spectral index α is parameterized as a power law $F_\nu \propto \nu^{-\alpha}$, where F_ν is the flux density at the frequency ν. Particularly, we accepted the day with at least three daily simultaneous data in all the four bands to ensure the reliability of the spectral index fitting. The spectral indices curve has been presented at the bottom panel of Fig. 1, where there are 90 spectral indices ranging from 0.068 (MJD 55668) to 3.79 (MJD 56680), with an averaged value of 1.23 and a standard deviation of 0.51. Note that the *V*-band light curve is not included in Fig. 1, because there is only one observation performed on MJD 56526 and a 'one-point' light curve makes no sense.

Light curves are significantly correlated, especially in the well-sampled *R* and *J* bands, and show prominent activities during the period of more than 4 years' monitoring. With linear regression, we obtain a strong correlation between F_R and F_J, with a correlation coefficient $r = 0.97$, a slope of the regression $B = 2.83 \pm 0.06$ and a chance probability $P < 10^{-4}$. Moreover, the flux densities in *BRJK* bands have a dramatic change, decreasing from January 2011 to May 2011, then passing into a fluctuating state at lower level. We also calculated the fractional variability amplitude $F_{\rm var}$ introduced by Edelson *et al.* (2002) to estimate the total variability of each curve. The $F_{\rm var}$ is defined as

$$F_{\rm var} = \sqrt{\frac{S^2 - \overline{\sigma_{\rm err}^2}}{\overline{x}^2}}, \tag{1}$$

where S^2 is the variance, $\sigma_{\rm err}$ the observational uncertainty, and $\overline{x}$ the mean value of the data of N measurements. The mean values and the $F_{\rm var}$ of light curves and spectral indices curve are listed in Table 1. Generally, the average fluxes increase from the *B* band to the *K* band, which is a common feature of blazars. Moreover, $F_{\rm var}$ in the optical–IR bands increases with wavelength if taking account of $F_{\rm var}$(*B*-band) *vs.* $F_{\rm var}$(*K*-band) and $F_{\rm var}$(*R*-band) *vs.* $F_{\rm var}$(*J*-band), which covered the same time range. This potential wavelength-dependent trend, suggesting the optical bands are fainter and vary less than the IR bands, might result from the facts that the synchrotron emission of this source peaks in optical–IR and a thermal component from the accretion disk varying on longer timescales is involved in the dominated jet emission, which is consistent with the variability amplitude analysis performed by Bonning *et al.* (2012), who suggest that the variability amplitude of FSRQs increases towards IR bands, indicating the presence

[1] http://www.astro.yale.edu/smarts.

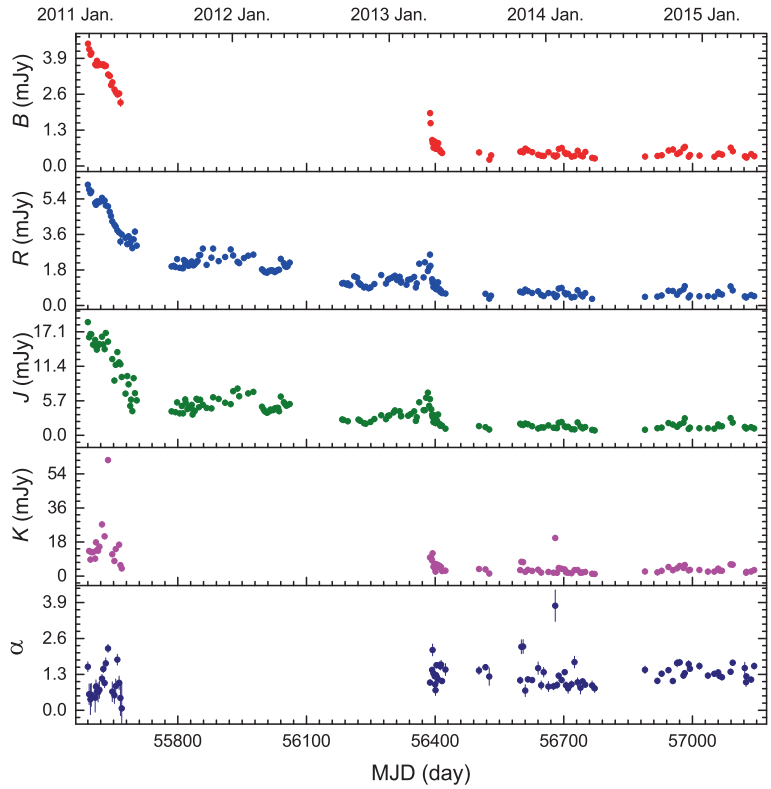

Figure 1. SMARTS optical–IR light curves of PKS 0537–441 in 2011–2015 after correction for Galactic extinction, and the bottom panel shows the corresponding spectral indices curve.

Table 1. Fractional variability amplitudes $F_{\rm var}$s and averaged flux densities in the *B*, *R*, *J* and *K* band (the statistics of spectral indices curve are also listed).

Band	Average flux (mJy)	$F_{\rm var}$
B	1.23 ± 0.01	1.06 ± 0.08
R	1.82 ± 0.02	0.76 ± 0.04
J	4.73 ± 0.05	0.87 ± 0.04
K	6.55 ± 0.08	1.20 ± 0.06
α	1.23 ± 0.18	0.37 ± 0.03

of some coherence between LBLs and FSRQs besides the similar peak frequency location of the synchrotron bump in these two subclasses of blazars.

Nevertheless, it is improper to compare $F_{\rm var}$ for all the four bands due to the lack of observations during MJD 55668–56386 in the *B* and *K* bands (see Fig. 1). If the data during this period in the *R* and *J* bands are subtracted, the $F_{\rm var}$s become 1.09 ± 0.08 in the *R* band and 1.18 ± 0.09 in the *J* band, suggesting $F_{\rm var}$s in different bands match with each other within error, which is perhaps because the observations during MJD 55668–56386 have a relatively weaker variability amplitude. Moreover, we also note that $F_{\rm var}$ values are higher than previously found for this sources (e.g., Li *et al.* 2015). This result may be somehow related to the quasi-monotonic light curve decreasing trend. Furthermore, the current daily data do not allow for searching of short-term variability.

3. Spectral behaviours

As can be seen from Fig. 1, there is no persistent trend between multicolor light curve and spectral indices exhibiting a large dispersion. In Fig. 2, we derived the spectral indices as a function of fluxes averaged over *BRJK* bands for the whole campaign: $\alpha = (1.27 \pm 0.05) - (0.01 \pm 0.01) F_{ave}$, with a correlation coefficient of $r = -0.02$ and a chance probability of $P = 0.77$, indicating that there is no overall correlation between spectral indices and average fluxes, which is in accordance with the long-term achromatic trend reported in Li *et al.* (2015) for this source. In all correlation analyses between spectral indices and brightness, the errors in both α and brightness were taken into account. Then, we divided the long-term spectral curve and light curves into small segments without a big observational gap (about 3 or 4 months) but covering the same time interval, and applied the linear regression to each pair of

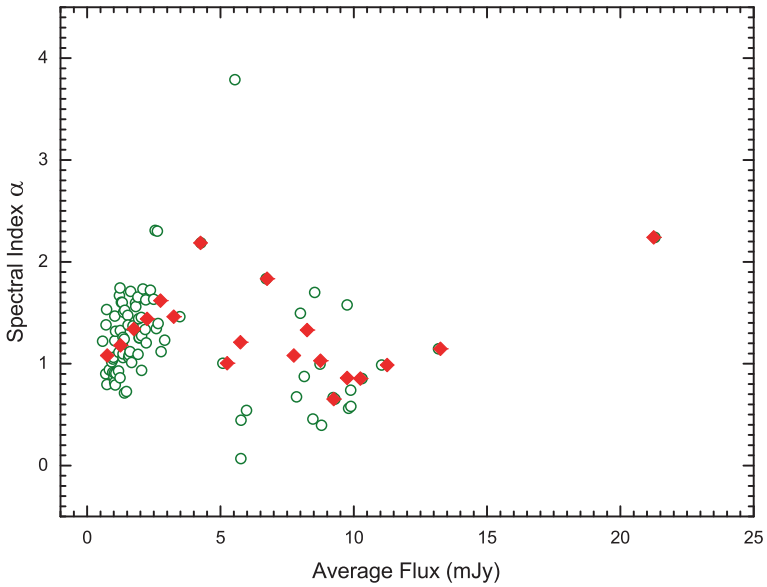

Figure 2. Relationship between spectral index α and average fluxes of all bands. Filled diamonds represent the mean values of α with a flux bin of 0.5 mJy.

segments to investigate the correlation between spectral indices and average fluxes in shorter timescales. Our results show that a linear regression correlation coefficient $r = 0.34$ and a slope of the regression $B = 0.05$ with chance probability $P = 0.06$ in MJD 55590–55704; $r = 0.54$ and $B = 0.20$ with $P < 10^{-4}$ in MJD 55785–56060; $r = 0.21$ and $B = 0.05$ with $P = 1.67$ in MJD 56183–556424; $r = 0.91$ and $B = 0.63$ with $P < 10^{-4}$ in MJD 56598–56772; $r = 0.29$ and $B = 0.12$ with $P = 0.17$ in MJD 56889–57143. This implies a modest positive correlation between spectral indices and flux densities in short-term timescales and indicates that the spectra become steeper when the fluxes increase, namely, a steeper-when-brighter or redder-when-brighter (RWB) behaviour.

Furthermore, considering the scattered distribution of spectral indices, we averaged the spectral indices with a flux bin of 0.5 mJy and plotted them in Fig. 2 with filled diamonds to evaluate the spectral evolution in more detail. A visual inspection of Fig. 2 indicates a complex relationship between average fluxes and spectral indices at different flux levels. The spectral indices increase as the fluxes increase at 0–4.5, 5–7 and 9–22 mJy flux levels, and decrease when the fluxes increase at 7–9 mJy level, which reveals that the spectrum exhibits different behaviours when PKS 0537–441 lies in different brightness states. This implies that the spectra become steeper (i.e., redder) when the fluxes increase at 0–4.5, 5–7 and 9–22 mJy flux levels, while the spectra become flatter (i.e. bluer) when the fluxes increase at 7–9 mJy level, namely BWB behaviour. On the basis of the REM IR/optical observations, Zhang *et al.* (2013) revealed that the spectrum steepens as the fluxes increase in the low state and flattens as the fluxes decrease in the high state, while Sandrinelli *et al.* (2014) reported a $R - H$ *vs.* H color-intensity plot with a general trend indicating bluer colour for decreasing flux. However, apart from a long-term achromatic trend and a mild RWB trend in short-term timescales, our analyses indicate the existence of a multiple spectral behaviour at different flux levels rather than a simple high or low-level division behaviour.

Generally, significant BWB and RWB trends for blazars have been investigated by several authors on diverse timescales (e.g., Gu *et al.* 2006; Rani *et al.* 2010; Agarwal *et al.* 2015). The superpositions of blue emission component from the Doppler-boosted relativistic jet, red component arising from the accretion disc, and/or geometric effects might be responsible for the different spectral changes in blazars (e.g., Gaur *et al.* 2012; Gupta *et al.* 2017). According to Villata *et al.* (2002, 2004), a long-term mild chromatic trend could be due to the variations of Doppler factor caused by the changes of the jet viewing angle, i.e., a change of Doppler factor on a power law spectrum does not imply a colour variation, which seems to be associated with our long-term achromatic trend. Moreover, a short-term 'strongly chromatic' trend should be resulted from the intrinsic processes related to jet emission mechanism and caused by particle acceleration in the jets (e.g., Kirk *et al.* 1998; Mastichiadis & Kirk 2002).

Spectral behaviour might also be accommodated within shock-in-jet models that can produce different fluctuations at different colors (e.g., Marscher 1996; Rani *et al.* 2010; Ikejiri *et al.* 2011; Gaur *et al.* 2012, and reference therein.). A relativistic shock propagating down the jet will accelerate electrons even to relativistic velocities and then trigger a flare. Emission at different frequencies is produced at different distances behind the shocks. The emission at higher frequencies will emerge sooner than that at lower frequencies, which gives a flatter spectrum during the early rising phase of the flare. Due to the energy losses of the high-frequency radiation, a more enhanced low-frequency flux will be observed and a steeper spectrum will show up during the later phases of the same flare (e.g., Agarwal & Gupta 2015). Therefore, a BWB trend usually tends to be apparent in BL Lac objects whose radiation is dominated by the non-thermal emission from the jet, e.g., BL Lacertae, S5 0716+714, 3C 66A and OJ 287 usually follow this trend (e.g., Villata *et al.* 2002; Carini *et al.* 1992; Ghosh *et al.* 2000; Ghisellini *et al.* 1997; Gu *et al.* 2006; Fan *et al.* 2011, and references therein), while a RWB indicating the spectrum becomes redder when brighter should be more likely to be seen in FSRQs, which is consistent with that the contribution from the luminous accretion disk is stronger towards the UV band underlying the variable jet emission, e.g., 3C 454.3 and PKS 0420–014 (e.g., Gu *et al.* 2006; Villata *et al.* 2006).

However, using the SMARTS data, Bonning *et al.* (2012) studied 12 blazars and reported that the blazar PKS 1510–089, PKS 2215–304, OJ 287 and AO 0235+164 exhibit complicated and anomalous behaviour rather than a simple chromatic/achromatic behaviour or a simplex BL lacs/FSRQs-division behaviour. We also note that, recently, Agarwal *et al.* (2015) reported a flattening trend of optical spectra with increasing fluxes in two FSRQs (3C 454.3 and 3C 279) and one BL Lac (S5 0716+714) on diverse timescales, and suggested that this trend was associated with a hardening of underlying non-thermal electron distribution; Agarwal and Gupta (2015) presented a dominant BWB trend that the spectra of BL Lacertae get flatter as the source becomes brighter on intra-night timescale; Gupta *et al.* (2017) found that OJ 287 did not show any significant spectral variation on long- or short-term timescales on the basis of the multiband optical photometric observations.

In our analysis, the relation between average fluxes and spectral indices reveals the existence of a long-term achromatic trend, a mild RWB trend on short-term timescales and a multiple spectral behaviour at different flux levels, which seems to be abnormal for a BL Lac object but partially due to the characteristics of the multi-band light curves that this source tended to be in a fluctuating state at a lower flux level after a dramatic decrease, as shown in Fig. 1. Nevertheless, this situation also could be explained by the shock-in-jet scenario discussed above. Furthermore, according to a new classification proposed by Ghisellini *et al.* (2011), PKS 0537–441 is considered as a transition source with SED properties that lie in between the BL Lac and FSRQ classes, where the broad emission lines with small equivalent width are relatively weak, providing a plausible explanation.

4. Cross-correlation analysis

In order to investigate the cross-correlations between different light curves and between light curves and spectral indices curve, we used the discrete correlation function (DCF) method introduced by Edelson and Krolik (1988). We first calculate the set of unbinned discrete correlation functions (UDCFs):

$$UDCF_{ij} = \frac{(a(i) - \overline{a})\,(b(j) - \overline{b})}{\sqrt{\sigma_a^2\,\sigma_b^2}}, \tag{2}$$

with the given data series a and b. Here, $a(i)$ and $b(j)$ are the individual points data series a and b respectively; $\bar{a}$ and $\bar{b}$ the means of the magnitudes and colour indices, and σ_a^2 and σ_b^2 their variances respectively. The DCF does not give a bin size automatically, therefore suitable time bins need to be sized after calculation of the UDCF. Then, the DCF can be calculated from the $UDCF_{ij}$ using

$$DCF(\tau) = \frac{1}{M}\sum UDCF_{ij}(\tau), \tag{3}$$

where τ is the centre of a time bin and M the total number of points in each bin. The standard error for each bin can be obtained via

$$\sigma(\tau) = \frac{1}{M-1}\sqrt{\sum\left[UDCF_{ij}(\tau) - DCF(\tau)\right]^2}. \tag{4}$$

With a DCF bin size of 10 d, the cross-correlation analysis between B-band and K-band light curves is plotted in Fig. 3 with olive-filled squares. The position of the DCF peak implies the possible time delay between two bands, and a negative time-delay corresponds to the case that the former band flux leads the latter, while a positive delay indicates the opposite. Figure 3 shows that the DCF value at time delay $\tau = 0$ is 0.56 ± 0.07, and a DCF maximum appears at a time delay between -40 and -20 d with a DCF

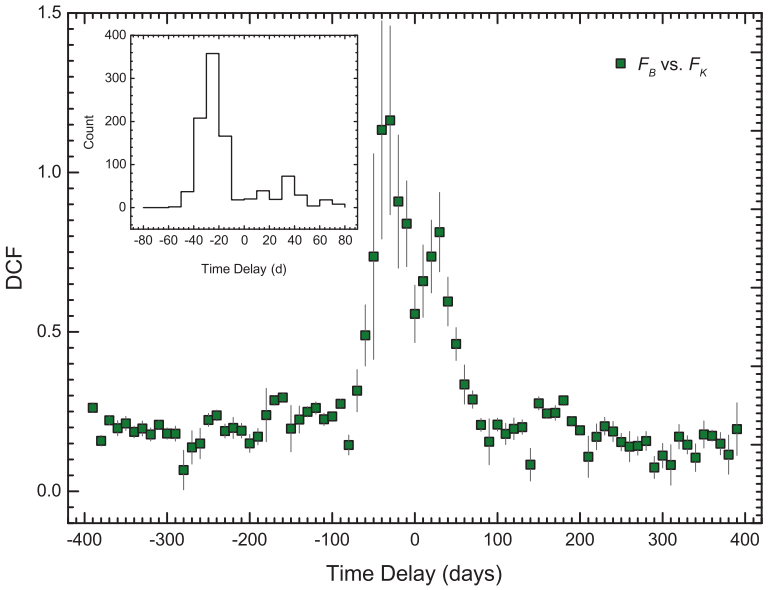

Figure 3. Example of the cross-correlation analyses for multi-band light curves and spectral indices. The olive-filled squares show the F_B *vs.* F_K, the inset shows the centroid distribution performed by 1000 FR/RSS realizations.

value of 1.16 ± 0.28, which indicates a positive correlation, and flux variations in the B band led those in the J band. Similar results were obtained when a wide range of DCF bin size were used, although a bigger bin size corresponded to a smoother DCF plot. We then employed Monte Carlo simulation technique, known as 'flux redistribution/random subset selection' (FR/RSS, Peterson *et al.* 1998) to obtain meaningful value and estimate the uncertainty for the time delays. After preforming 1000 FR/RSS Monte Carlo realizations, we obtained the cross-correlation centroid distribution (CCCD), in which the centroid is given by $\tau_c = (\Sigma_i \tau_i DCF_i)/(\Sigma_i DCF_i)$, where sums run over the points which have a DCF value close to the peak ($DCF_i > 0.8 DCF_{\rm peak}$). Then, the time delay and the uncertainties of -29 ± 10 days are derived from the CCCD (see the inset of Fig. 3) at 1σ confidence level, which may indicate that the B-band flux precedes the J-band flux by about 30 d.

We also applied the DCF technique to analyse the correlation between each pair of the B-, R-, J-, K-band light curves using the same procedure, and have presented the results in Table 2. Except that the DCF analysis for R *vs.* J yields a broad DCF peak at time delay of 15 d with large uncertainty, most of the DCF plots (high-frequency band *vs.* low-frequency band) give a similar shape, namely, DCF maximums appear at time delays between -40 and -10 d with positive DCF values, indicating that the lower-frequency variabilities generally follow the higher-frequency ones, which is a common feature for blazars. If the particle acceleration processes occur in the inner jet and the optical–IR flare emission is produced in shocks propagating down the jet, it is expected that the synchrotron emissions in optical and IR bands originate from the same region, where the high-energy photons emerge sooner and closer to the shock front than the lower-frequency radiation, resulting in spectral changes as discussed in section 3

Table 2. Possible time delays determined by the DCF method. Time delays and uncertainties are derived at 1σ confidence level by FR/RSS Monte Carlo technique. DCF values at time delay $\tau = 0$ are also displayed.

Cross-correlation	Time delay (days)	$\mathrm{DCF}_{\tau=0}$
B *vs.* R	-28 ± 8	1.35 ± 0.08
B *vs.* J	-26 ± 8	1.33 ± 0.13
B *vs.* K	-29 ± 10	0.56 ± 0.07
R *vs.* J	15 ± 16	0.99 ± 0.13
R *vs.* K	-23 ± 9	0.74 ± 0.09
J *vs.* K	-28 ± 8	0.69 ± 0.13
$F_{\rm var}$ *vs.* α	21 ± 10	-0.34 ± 0.07

The cross-correlation analysis between the spectral indices and average fluxes $F_{\rm ave}$ has been demonstrated in Fig. 4 with blue-filled circles, which shows a different characteristic from the DCF analysis for F_B *vs.* F_K. The DCF plot reveals a negative correlation between α and $F_{\rm ave}$ with a DCF minimum of -0.69 ± 0.17 at a time delay between 10 and 30 d, and the FR/RSS procedure yields a time delay of 21 ± 10 d at 1σ confidence level, indicating that the spectral changes precede the

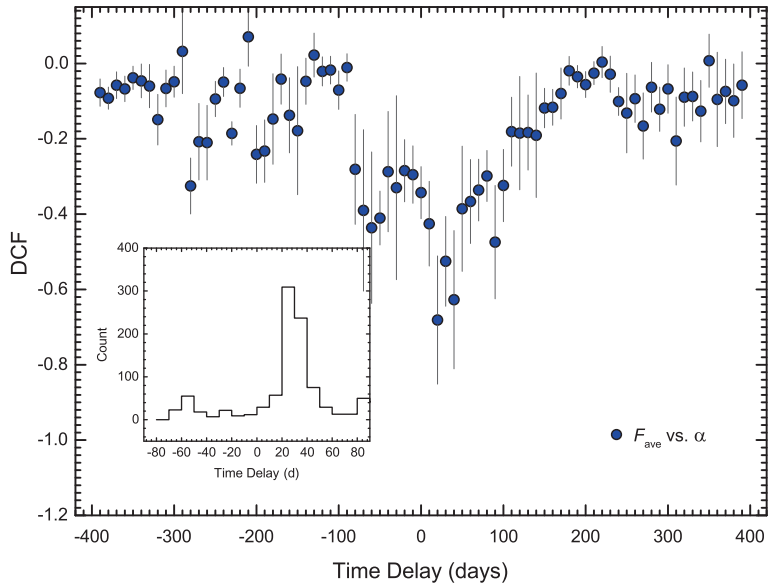

Figure 4. Same as Fig. 3, but for F_{ave} *vs.* α (blue-filled circles).

flux variations by a few weeks with a negative correlation. The energy-dependent time delays and hysteresis pattern between spectra and fluxes observed in this source seem to be associated with the complex spectral behaviour, i.e., the existence of a long-term achromatic trend, a mild RWB trend in short-term timescales and a multiple spectral behaviour at different flux levels, and shed some light on the investigations of particle acceleration, synchrotron cooling and flux variability timescales for blazars.

5. Summary

The well-studied blazar PKS 0537–441 has been observed by the SMARTS 1.3 m telescope from 2011 to 2015. We have reconcentrated on the simultaneous and homogeneous optical–IR variability in a duration of about 1600 d. Well-correlated light curves in the *BRJK* bands, and the corresponding spectral indices are reported, and all the curves show prominent activities. If considering the same time coverage of light curves in different bands, the F_{var} and average fluxes in the optical–IR bands seem to increase with wavelength, indicating that some potential coherence exists between LBLs and FSRQs and the dominant jet emission might involve the thermal contribution from a more slowly varying disk.

There is no persistent trend between multiband light curve and spectral indices on long-term timescales, consistent with the variations of Doppler factor on a power law spectrum. However, after dividing the long-term spectral curve and light curves into small segments without a big observational gap and evaluating the spectral evolution in a flux level pattern, we found a mild RWB trend on short-term timescales and a multiple spectral behaviour at different flux levels, which could be generally explained by the shock-in-jet scenario. By means of the DCF technique, we found the spectral changes precede the flux variations by a few weeks with a negative correlation, and a common feature for blazars that the lower-frequency variabilities follow the higher-frequency ones, which indicates that the optical–IR synchrotron emission is produced in the same region where the spectral changes occur , and seem to be associated with the complex spectral behaviour.

Acknowledgements

This work is supported by the Science Research Project of Education Department of Yunnan Province, China (2017ZZX079, 2016ZZX230), and the Youth Program of the Applied Basic Research Projects of Yunnan Province, China (2017FD147). This paper has made use of up-to-date SMARTS optical/near-infrared light curves that are available at www.astro.yale.edu/smarts/glast/home.php.

References

Agarwal A., Gupta A. C. 2015, Mon. Not. R. Astron. Soc., 450, 541

Agarwal A., Gupta A. C., Bachev R. et al. 2015, Mon. Not. R. Astron. Soc., 451, 3882

Bessell M. S., Castelli F., Plez B. 1998, Astron. Astrophys., 333, 231
Bonning E., Urry C. M., Bailyn C. et al. 2012, Astrophys. J., 756, 13
Böttcher M. 2007, Astrophys. Space Sci., 309, 95
Cardelli J. A., Clayton G. C., Mathis J. S. 1989, Astrophys. J., 345, 245
Carini M. T., Miller H. R., Noble J. C., Goodrich B. D. 1992, Astron. J., 104, 15
Celotti A., Ghisellini G., Fabian A. C. 2007, Mon. Not. R. Astron. Soc., 375, 417
D'Ammando F., Antolini E., Tosti G. et al. 2013, Mon. Not. R. Astron. Soc., 431, 2481
Edelson R., Turner T. J., Pounds K. et al. 2002, Astrophys. J., 568, 610
Edelson R. A., Krolik J. H. 1988, Astrophys. J., 333, 646
Fan J. H., Liu Y., Li Y. et al. 2011, J. Astrophys. Astr., 32, 67
Gaur H., Gupta A. C., Strigachev A. et al. 2012, Mon. Not. R. Astron. Soc., 425, 3002
Ghisellini G., Villata M., Raiteri C. M. et al. 1997, Astron. Astrophys., 327, 61
Ghisellini G., Tavecchio F., Foschini L., Ghirlanda G. 2011, Mon. Not. R. Astron. Soc., 414, 2674
Ghisellini G., Tavecchio F., Maraschi L., Celotti A., Sbarrato T. 2014, Nature, 515, 376
Ghosh K. K., Ramsey B. D., Sadun A. C. 2000, Astrophys. J. Suppl. Ser., 127, 11
Gu M. F., Lee C.-U., Pak S., Yim H. S., Fletcher A. B. 2006, Astron. Astrophys., 450, 39
Gupta A. C., Agarwal A., Mishra A. et al. 2017, Mon. Not. R. Astron. Soc., 465, 4423
Ikejiri Y., Uemura M., Sasada M. et al. 2011, Publ. Astron. Soc. Japan, 63, 639
Impiombato D., Covino S., Treves A. 2011, Astrophys. J. Suppl. Ser., 192, 12
Kirk J. G., Rieger F. M., Mastichiadis A. 1998, Astron. Astrophys., 333, 452
Li X., Zhang L., Luo Y., Wang L., Zhou L. 2015, Mon. Not. R. Astron. Soc., 449, 2750
Li X.-P., Luo Y.-H., Zhang L., Yang C., Yang H.-T., Cai Y. 2017, Mon. Not. R. Astron. Soc., 464, 3972
Mannheim K. 1998, Science, 279, 684
Maraschi L., Ghisellini G., Celotti A. 1992, Astrophys. J. Lett., 397, 5
Marscher A. P. 1996, in Astron. Soc. Pacific. Conf. Ser., Vol. 110, 248
Mastichiadis A., Kirk J. G. 2002, Publ. Astron. Soc. Aust., 19, 138
Peterson B. M., Wanders I., Horne K. et al. 1998, Publ. Astron. Soc. Pacific, 110, 660
Pian E., Falomo R., Hartman R. C. et al. 2002, Astron. Astrophys., 392, 407
Rani B., Gupta A. C., Strigachev A. et al. 2010, Mon. Not. R. Astron. Soc., 404, 1992
Sandrinelli A., Covino S., Treves A. 2014, Astron. Astrophys., 562, 79
Sandrinelli A., Covino S., Treves A. 2016, Astrophys. J., 820, 20
Schlafly E. F., Finkbeiner D. P. 2011, Astrophys. J., 737, 103
Ulrich M.-H., Maraschi L., Urry C. M. 1997, Annu. Rev. Astron. Astrophys., 35, 445
Urry C. M., Padovani P. 1995, Publ. Astron. Soc. Pacific, 107, 803
Villata M., Raiteri C. M., Kurtanidze O. M. et al. 2002, Astron. Astrophys., 390, 407
Villata M., Raiteri C. M., Kurtanidze O. M. et al. 2004, Astron. Astrophys., 421, 103
Villata M., Raiteri C. M., Balonek T. J. et al. 2006, Astron. Astrophys., 453, 817
Zerbi R. M., Chincarini G., Ghisellini G. et al. 2001, Astron. Nach., 322, 275
Zhang B.-K., Wang S., Zhao X.-Y., Dai B.-Z., Zha M. 2013, Mon. Not. R. Astron. Soc., 428, 3630